



Published in final edited form as:

Nat Med. 2013 December ; 19(12): 1643–1648. doi:10.1038/nm.3400.

Ammonia triggers neuronal disinhibition and seizures by impairing astrocyte potassium buffering

Vinita Rangroo Thrane^{1,2,3,5}, Alexander S Thrane^{1,2,3,5}, Fushun Wang¹, Maria L Cotrina¹, Nathan A Smith^{1,4}, Michael Chen¹, Qiwu Xu¹, Ning Kang¹, Takumi Fujita¹, Erlend A Nagelhus^{1,2}, and Maiken Nedergaard¹

¹Division of Glial Disease and Therapeutics, Center for Translational Neuromedicine, University of Rochester, NY 14642, USA

²Center for Molecular Medicine Norway and Letten Centre, Institute for Basic Medical Sciences, University of Oslo, Oslo 0317, Norway

³Department of Ophthalmology, Haukeland University Hospital, Bergen 5021, Norway

⁴Laboratory of Glial-Neuronal Interactions in Epilepsy, The Brain Institute, University of Utah, UT 84112, USA

Abstract

Ammonia is a ubiquitous waste product of protein metabolism that can accumulate in numerous metabolic disorders, causing neurological dysfunction ranging from cognitive impairment to tremor, ataxia, seizures, coma and death¹. The brain is especially vulnerable to ammonia as it readily crosses the blood-brain barrier in its gaseous form, NH₃, and rapidly saturates its principal removal pathway located in astrocytes². Thus, we wanted to determine how astrocytes contribute to the initial deterioration of neurological functions characteristic of hyperammonemia *in vivo*. Using a combination of two-photon imaging and electrophysiology in awake head-restrained mice, we show that ammonia rapidly compromises astrocyte potassium buffering, increasing extracellular potassium concentration and overactivating the Na⁺-K⁺-2Cl⁻ cotransporter isoform 1 (NKCC1) in neurons. The consequent depolarization of the neuronal GABA reversal potential (E_{GABA}) selectively impairs cortical inhibitory networks. Genetic deletion of NKCC1 or inhibition of it with the clinically used diuretic bumetanide potently suppresses ammonia-induced neurological dysfunction. We did not observe astrocyte swelling or brain edema in the acute phase, calling into question current concepts regarding the neurotoxic effects of ammonia^{3,4}.

Users may view, print, copy, download and text and data- mine the content in such documents, for the purposes of academic research, subject always to the full Conditions of use: http://www.nature.com/authors/editorial_policies/license.html#terms

Correspondence should be addressed to A.S.T. (alexander.thrane@gmail.com).

⁵These authors contributed equally to the paper.

Note: Any Supplementary Information and Source Data files are available in the online version of the paper.

AUTHOR CONTRIBUTIONS

V.R.T., A.S.T., E.A.N., M.L.C. and M.N. planned the project. V.R.T., A.S.T., M.L.C., E.A.N. and M.N. wrote the manuscript. V.R.T. and A.S.T. performed *in vivo* electrophysiology, imaging and data analysis. F.W., N.K. and Q.X. performed *in situ* electrophysiology. A.S.T., V.R.T. and M.C. performed behavioral experiments. A.S.T., V.R.T. and Q.X. performed *in situ* imaging. N.A.S. performed rubidium experiments. T.F. performed ATPase experiments. M.L.C. performed immunohistochemistry.

COMPETING FINANCIAL INTEREST

The authors declare that there are no competing financial interests.

Instead, our findings identify failure of potassium buffering in astrocytes as a crucial mechanism in ammonia neurotoxicity and demonstrate the therapeutic potential of blocking this pathway by inhibiting NKCC1.

Ammonia neurotoxicity is an almost universal phenomenon that occurs in all animals from fish to humans⁵. Ammonia homeostasis is uniquely important in the brain as equimolar NH_4^+ is released with glutamate during neuronal firing⁶. Interestingly, the enzyme that removes ammonia and glutamate, glutamine synthetase, has a higher affinity for ammonia than this excitotoxic neurotransmitter^{2,7}. Mortality in ammonia-handling disorders is primarily due to acute episodes of elevated blood ammonia (hyperammonemia), characterized by stupor, seizures and coma, which are the main focus of our study¹. Ammonia was also recently identified as an independent contributor to seizure development in epileptic children with normal urea cycle function⁸. To understand this phenomenon we wanted to study the early effect of ammonia on intact nervous tissue, both avoiding the adaptive changes associated with chronic exposure and also any ammonia-independent pathology accompanying overt liver failure^{9,10}.

To induce acute ammonia intoxication we subjected awake adult ornithine transcarbamylase (OTC) deficient or *Otc^{spf-ash}* mice to an intra-peritoneal ammonia load (ammonium chloride or acetate, 7.5 mmol kg^{-1}) (Fig. 1a)⁹. OTC deficiency is a childhood urea cycle disorder characterized by a reduced ability to metabolize ammonia to urea in the liver¹. Shortly after the injection we recorded a brisk increase in extracellular ammonia concentration ($[\text{NH}_4^+]_o$) from 0.54 ± 0.18 to $4.83 \pm 0.52 \text{ mM}$ in brain and to $4.21 \pm 0.59 \text{ mM}$ in plasma (Supplementary Fig. 1a–b). We employed several behavioral measures to track the progression and severity of ammonia neurotoxicity. Automated video tracking revealed an early decrease in spontaneous movement (13.69 ± 1.48 vs. $0.42 \pm 0.22 \text{ m min}^{-1}$) (Fig. 1b). We also developed a phenotype severity score that allowed us to track the rapid onset of neurological dysfunction (0.53 ± 0.28 vs. 9.00 ± 0.46) (Fig. 1c)⁹. Similar to children with inborn OTC deficiency, the *Otc^{spf-ash}* mice also displayed impaired learning prior to receiving the ammonia load, likely reflecting the baseline excess of $[\text{NH}_4^+]_o$ (*Otc^{spf-ash}* 0.32 ± 0.07 vs. wild-type $0.074 \pm 0.014 \text{ mM}$ in plasma) (Fig. 1d, Supplementary Fig. 1c)^{1,9,11}

In addition to cognitive, sensory, and motor impairment, children with OTC deficiency typically develop myoclonic and other types of generalized seizures during episodes of hyperammonemia¹. Around weaning *Otc^{spf-ash}* mice also developed spontaneous myoclonuses, which are brief (< 2 s) involuntary jerky movements caused by cortical seizure activity⁹. We used an ammonia challenge to precipitate a more robust seizure phenotype and found that intermediate doses triggered numerous myoclonic seizures, whilst a lethal dose induced longer lasting generalized tonic-clonic seizures (Fig. 1e, Supplementary Video 1). We found that the frequency of myoclonic seizures closely correlated with overall phenotype severity, and both were entirely masked by anesthesia, emphasizing both the clinical relevance of our model and the need for recordings in awake animals (Fig. 1f).

We next asked whether a primary dysfunction of astroglia might mediate the neurotoxic effects of ammonia. Astrocytes possess the primary enzyme necessary for ammonia

detoxification, and are consequently subject to more than 4-times as much ammonia influx as any other cell type in the brain¹². The current literature suggests that astrocyte swelling and brain edema are necessary for ammonia neurotoxicity, but consists mainly of *ex vivo* and *post mortem* studies in the late stages of liver coma². Using *in vivo* two-photon imaging we found that these features were associated with the immediate neurotoxic phenotype⁴, but instead found a transient astrocyte shrinkage of $5.04 \pm 0.85\%$ in both wild-type and *Otc^{spf-ash}* mice (Fig. 2a,b)¹³. Astrocyte swelling and brain edema were only elicited in terminal stages of ammonia neurotoxicity (Supplementary Fig. 1d, e)¹⁰. Additionally, deletion of the astrocyte water channel aquaporin-4 (AQP4) did not ameliorate the neurological dysfunction (Supplementary Fig. 1f)^{14,15}. We then proceeded to test the effect of ammonia neurotoxicity on the principal mode of astrocyte signaling - intracellular calcium transients. We found that ammonia intoxication caused increased and desynchronized astrocyte calcium signaling, which were temporally correlated with the seizure phenotype (calcium transient frequency 2.67 ± 0.36 vs. 9.03 ± 1.16 Hz cell⁻¹ 10⁻³) (Fig. 2c, Supplementary Video 2, 3, Supplementary Fig. 1g-i)¹⁶.

Since the widespread increase in astrocyte calcium signaling could not be due to swelling¹⁵, we next asked whether it might be linked to the interference of ammonia with potassium transport previously described in cell culture and kidney^{4,6,17,18}. Using NH₄⁺ and K⁺ ion-sensitive microelectrodes (ISM)¹⁹ in awake *Otc^{spf-ash}* animals we found that systemic ammonia intoxication increased extracellular potassium ([K⁺]_o) by 1.93 ± 0.19 mM (subtracted for interference¹⁷, Fig. 2d). As previous studies and our results indicate that the bulk of ammonia neurotoxicity occurs in cortical grey matter (Supplementary Fig. 2a)^{2,20}, we next applied ammonia directly on the cortex of awake wild-type mice. The ammonia dose was titrated in initial experiments to achieve a [NH₄⁺]_o increase of 5.82 ± 0.18 mM, which was similar to our observations from systemic toxicity and sufficient to reproduce the seizure phenotype (Supplementary Table 1). We also found that cortical ammonia intoxication in wild-type mice increased [K⁺]_o by 2.24 ± 0.17 mM from a resting level of 3.91 ± 0.27 mM (pooled control data) (Fig. 2e, Supplementary Fig. 2b-d). The [K⁺]_o increase in both the systemic and cortical models were strongly correlated with and consistently preceded myoclonic seizures (systemic 4.91 ± 0.35 min and cortical 2.88 ± 0.20 min), and recovered on washout as the neurological manifestations subsided (Fig. 2f). Conversely, the pH effects of ammonia were mild, delayed and correlated poorly with clinical phenotype (Supplementary Fig. 2e).

Having established that ammonia increases [K⁺]_o sufficiently to cause neurological dysfunction *in vivo*, we proceeded to ask: Does the excess NH₄⁺ load on astrocyte membranes impair potassium buffering by inhibiting transport or directly competing for uptake? The gradients driving astrocyte uptake of potassium are largely dependent on Na⁺-K⁺-ATPase (NKA) activity, especially in the context of sustained [K⁺]_o elevations^{17,21,22}. Using biologically relevant concentrations of ammonia (0.5–10 mM), we demonstrated a dose-dependent reduction in NKA-mediated (ouabain-sensitive) potassium analogue rubidium (⁸⁶Rb⁺) uptake in cultured astrocytes (Fig. 2g, Supplementary Fig. 2f)²¹. We then substituted KCl with NH₄Cl in an astroglial NKA assay, and found that NH₄Cl alone was able to maintain normal NKA activity (Fig. 2g), indicating that NH₄⁺ competes with K⁺ for

transport. Notably, NH_4^+ and K^+ ions have a comparable hydrated radius and charge⁶. To test whether the $[\text{K}^+]_o$ increase alone is sufficient to reproduce the phenotype of ammonia neurotoxicity *in vivo*, we superfused KCl (12.5 mM) across the cortex of awake wild-type mice. The KCl superfusion increased $[\text{K}^+]_o$ by 2.37 ± 0.03 mM and caused the mice to develop myoclonic seizures equivalent to those seen in ammonia neurotoxicity (Fig. 2h). Combined, our observations indicate that ammonia short-circuits potassium transport in astrocytes, and that the consequent increase in $[\text{K}^+]_o$ alone is sufficient to lead to neurological dysfunction. Since astrocyte calcium transients potently stimulate NKA activity²¹, NKA activity is known to increase in hyperammonemia¹³, and increased NKA pumping causes cell shrinkage (3Na^+ export vs. 2K^+ import), we speculate that our imaging observations represent compensatory changes in astrocytes to buffer the excess substrate ($[\text{NH}_4^+]_o$ and $[\text{K}^+]_o$) (Fig. 2i).

How does impaired astrocyte potassium buffering lead to neurological dysfunction and seizures? Previous *ex vivo* studies have generated numerous conflicting hypotheses about the effect of ammonia on neurotransmission^{23–25}. To explore whether excess ammonia and potassium might cause neurological dysfunction by impairing cortical inhibition^{26,27} we employed paired-pulse whisker stimulation in awake wild-type mice. This paradigm elicits two successive field excitatory post-synaptic potentials (fEPSP), where the second fEPSP has lower amplitude primarily due to the activation of cortical inhibitory networks (quantified by a paired-pulse ratio (PPR) < 1)²⁸. We found that ammonia (or potassium) intoxication impaired cortical inhibition, illustrated by an increased PPR from 0.64 ± 0.13 (control) to 1.56 ± 0.24 (ammonia) and 1.48 ± 0.22 (potassium), which recovered to 0.61 ± 0.15 (washout) (Fig. 3a). To further explore the link between impaired astrocyte potassium buffering and neuronal disinhibition we then patched pyramidal neurons in acute cortical slices from wild-type mice. Initial experiments showed that adding 7 mM ammonia to the perfusate reproduced the increase in $[\text{NH}_4^+]_o$ and $[\text{K}^+]_o$ observed *in vivo* (3.67 ± 0.53 mM and 1.88 ± 0.13 mM respectively) (Fig. 3b). Next, using whole-cell recordings and γ -aminobutyric acid (GABA) application we found that ammonia depolarized E_{GABA} by $+12.33 \pm 3.66$ mV (Fig. 3c–e). This effect was GABA_A -receptor dependent, as GABA_A -receptor antagonist bicuculline completely blocked the GABA-induced current (Fig. 3f), but was not associated with any significant change in neuronal resting membrane potential or input resistance²⁵.

The inhibitory action of GABA_A -receptors is dependent on a hyperpolarized E_{GABA} , which in turn depends on the balance of chloride transport by NKCC1 and $\text{K}^+\text{-Cl}^-$ cotransporter isoform 2 (KCC2)²⁹. KCC2 deletion is known to cause lethal seizures immediately after birth due to excess chloride import via NKCC1³⁰. Conversely, deletion of the NKCC1 isoform *Slc12a2*, widely expressed in neurons and secretory epithelia, is associated with normal inhibitory GABA-ergic function^{31,32}. NKCC1 is thus the principal chloride importer in neurons, and inhibition, knock-out or knock-down of this transporter has been shown to treat temporal lobe, hypoglycemic, febrile and neonatal seizures by ensuring a hyperpolarized E_{GABA} ^{26,27,31–34}. Therefore, we next tested the diuretic bumetanide, a highly specific NKCC1 inhibitor at low concentrations^{26,27,35}. In our study, bumetanide treatment successfully prevented the depolarizing effect of ammonia on E_{GABA} (Fig. 3d, e).

To ensure the molecular specificity of bumetanide, we also performed gramicidin-perforated patch recordings in conditional NKCC1 knock-out (*Slc12a2^{-/-}*) and wild-type littermates (*Slc12a2^{+/+}*). NKCC1 deletion completely blocked the depolarizing effect of ammonia on E_{GABA} ($+11.14 \pm 1.22$ in wild-type and $+1.00 \pm 1.07$ in *Slc12a2^{-/-}*) (Fig. 3g, h). Supporting our observations, previous *in vivo*, *in situ* and *in vitro* work has shown that neurons exposed to elevated ammonia or potassium levels have significantly increased intracellular chloride content^{36,37}. Using immunohistochemistry of NKCC1 knock-out and wild-type mice we found that NKCC1 is present in cortex (Fig 3i), confirming previous studies indicating NKCC1 expression in adult brain, although at lower levels than in developing tissue^{26,38}. We also observed no obvious differences in the expression pattern of NKCC1 between wild-type and *Otc^{spf-ash}* mice. Taken together, our observations indicate that elevated $[NH_4^+]_o$ and $[K^+]_o$ drive an over-activation of neuronal NKCC1, leading to a depolarization of E_{GABA} , cortical disinhibition and seizures (Fig. 3j).

We proceeded to explore potential treatments for ammonia neurotoxicity (Fig. 4a). It has previously been suggested that reducing ammonia influx into astrocytes by inhibiting glutamine synthetase can improve clinical outcome³. However, in awake intact animals we found that this strategy only worsened neurological phenotype by increasing the overall $[NH_4^+]_o$ and $[K^+]_o$ load on neurons (Supplementary Fig. 3a–c). Similarly, blocking ammonia import into glia via potassium transporters would also promote seizure development^{17,22}. Instead, we hypothesized that inhibiting NKCC1 over-activation would be the most effective strategy, as this disrupts the vicious cycle of ammonia-induced disinhibition, excess neuronal firing, further potassium and ammonia release, and more disinhibition. Using the previously described paired-pulse paradigm, we found that bumetanide significantly improved disinhibition following cortical application of either ammonia or potassium (PPR 0.88 ± 0.15 following ammonia + bumetanide application, PPR 0.59 ± 0.17 after washout of both, PPR 0.92 ± 0.18 following KCl + bumetanide) in wild-type mice (Fig. 4b, Supplementary Fig. 3d). NKCC1 inhibition also increased spontaneous mouse movement (0.42 ± 0.22 to 3.17 ± 0.46 m min^{-1}), reduced the phenotype severity score (9.00 ± 0.46 to 6.00 ± 0.72) and decreased myoclonic seizure frequency (0.78 ± 0.05 to 0.13 ± 0.03 with cortical KCl, 1.02 ± 0.07 to 0.10 ± 0.02 with cortical ammonia and 2.66 ± 0.14 to 0.32 ± 0.02 seizures min^{-1} with systemic ammonia) (Fig. 4c, d). Moreover, survival of *Otc^{spf-ash}* mice after an ammonia overdose (10 mmol kg^{-1}) increased by a factor of 3.87 (hazard rate ratio 0.26, 95% confidence interval 0.08 to 0.87) (Fig. 4e). These clinically relevant improvements were observed both when bumetanide was administered systemically (30 mg kg^{-1} , 5 min prior to ammonia in *Otc^{spf-ash}* mice) and cortically (5 μ M in wild-type mice). Bumetanide is also routinely used in clinical practice, has a favorable side-effect profile³⁵, and is estimated to have ~33% blood-brain barrier penetration³⁹. Moreover, the therapeutic effect of bumetanide could not be attributed to a normalization of $[K^+]_o$, $[NH_4^+]_o$ or brain glutamine, which were unaltered by the treatment in both wild-type and *Otc^{spf-ash}* mice (Supplementary Table 2, Supplementary Fig. 3e, f).

In summary, we demonstrate that the immediate neurotoxic effects of ammonia are dependent on a breakdown of neuro-glial interplay involving two critical steps: (1) Ammonia competitively impairs astrocyte potassium buffering to such an extent that the

resultant increase in $[K^+]_o$ (~2 mM) alone is sufficient to generate neurological dysfunction and seizures in awake animals. (2) Excess $[NH_4^+]_o$ and $[K^+]_o$ drive an over-activation of NKCC1 that compromises inhibitory neurotransmission in the cortex, and a deletion or selective inhibition of NKCC1 potentially treats all the neurological manifestations of acute ammonia intoxication. Additionally, our results question the contribution of astrocyte swelling and brain edema to the onset of neurological dysfunction. The use of awake behaving mice proved critical as general anesthetics masked the clinical phenotype¹⁶. Our study thus provides a framework to further explore the clinical potential of NKCC1 inhibitors in treating the broad range of debilitating disorders of ammonia handling. Studies are also needed to investigate the role of this pathway in disorders characterized by chronic hyperammonemia and cognitive impairment.

ONLINE METHODS

Mice and breeding

Otc^{spf-ash} B6C3-F1, *Glt1-eGFP* BAC, *Slc12a2^{-/-}* SVJ129/blksw and *Aqp4^{-/-}* C57BL/6J mice were bred as described previously^{9,15,32,40}. For *in vivo* experiments males from 8–12 weeks were used. *Otc^{spf-ash}* mice were crossed with *Glt1-eGFP* mice for imaging experiments. Wild-type littermates of the appropriate strain were either bred or obtained from Jackson Laboratories, along with Wistar rat pups. All animal experiments were approved by the Animal Care and Use Committee of the University of Rochester.

Behavioral characterization

We developed a phenotype severity score to quantify the degree of ammonia neurotoxicity based on previous studies^{9,41,42}. Each animal was scored every 5–15 minutes for the following phenotypes: hyperacusis (0–2), imbalance (0–3), ataxia/tremor (0–3) and level of consciousness (0–3). A maximum score of 11 represents deep coma (no corneal reflex) whilst 0 represents normal wakefulness. Hyperacusis was scored 0 if the mouse did not display a startle response to 30–60 dB sound, 1 if the mouse responded to only 60 dB and 2 if it responded to 30 dB as well. Imbalance was scored using a ledge test, and the mice were given 0 if they balanced on the ledge and let themselves down in a controlled fashion, 1 if they lost their footing whilst walking on the ledge, 2 if they did not effectively walk on or let themselves down from the ledge, and 3 if they were unable to walk, get down, or simply fell off. Ataxia/tremor was scored using a gait test, where the mouse is encouraged to walk for a short distance. The mouse gets 0 if it walks effectively, 1 if it has a slight tremor, 2 if it has a broad based gait or severe tremor, 3 if it drags its abdomen on the ground or is unable to walk. Consciousness was scored as either 0 for awake, 1 loss of scatter reflex, 2 loss of righting reflex (LORR), 3 loss of corneal reflex. Automated movement analysis was performed using AnyMaze™ software analysis of CCD-camera recordings in a standard mouse cage. To analyze cognitive abilities, two commercial conditioning chambers (H10-11M-TC, Coulbourn Instruments) were adapted for contextual fear conditioning. Over the course of 4 days, mice were trained via a tone/shock protocol and trained to fear contextual and auditory cues^{43–45}. Better-trained mice exhibited higher freezing percentages in the presence of auditory or contextual cues.

Animal preparation for awake *in vivo* recordings

Mouse preparation was modified from published protocols^{46,47}. Briefly, mice were anesthetized using isoflurane (1.5% mixed with 1–2 L min⁻¹ O₂), head restrained with a custom-made mini-frame and habituated to the restraint over 2 days in multiple sessions, with a total training duration of 3–4 hours. A 1.5 mm craniotomy was then opened over the somatosensory cortex (1.5 mm in diameter, 3 mm lateral and 1.5 mm posterior to the bregma), the dura was carefully removed, and the mice were allowed 60 min recovery prior to conducting the experiments. The craniotomy procedure lasted < 20 min to minimize anesthesia exposure on the recording day. Animals were then head-restrained, placed in a behavioral tube to minimize movement and relocated to the imaging room, which was kept dark and quiet. Body temperature was maintained with a heating pad. For systemic drug treatment, a polyethylene intraperitoneal (i.p.) catheter was surgically implanted using a Seldinger technique to deliver drugs accurately and with minimal manipulation. For cortical drug application artificial cerebrospinal fluid (aCSF) was perfused across the cortex of awake mice at a rate of 2 mL min⁻¹, into a custom-made well with ~200 µL volume, through tubing with ~100 µL volume, meaning the entire volume bathing the brain was exchanged every ~ 9 s. The aCSF solution contained (in mM) 126 NaCl, 2.5 KCl, 1.25 NaH₂PO₄, 2 MgCl₂, 2 CaCl₂, 10 glucose, and 26 NaHCO₃, pH 7.4. For imaging, calcium indicator rhod-2 AM (Invitrogen, 2 mM) was loaded onto exposed cortex for 30–40 min before applying agarose (1.5%, type III-A, Sigma) and a coverslip¹⁵.

Electrophysiological recordings

In vivo and *in situ* recordings were obtained from layer II somatosensory cortex, and coronal cortical slices were prepared from P21–30 mice. Ion-sensitive microelectrodes (ISM) for K⁺, NH₄⁺ and H⁺ were pulled from double-barreled pipette glass (PB150-6, WPI) with a tip diameter of 1–3 µm. The pipettes were silanized (coated) with dimethylsilane I (Fluka, Sigma) and filled with either K⁺ ionophore I cocktail B (Fluka, selectivity coefficient $-1.8 \log(K^+/NH_4^+)$), NH₄⁺ ionophore I cocktail B (Fluka, $-0.9 \log(NH_4^+/K^+)$) or H⁺ ionophore I cocktail A (Fluka, Sigma). The backfill solutions for the K⁺, NH₄⁺ and H⁺ ISMs were 0.15 M KCl, 0.5 M NH₄Cl and phosphate-buffered saline (PBS) with a pH of 7.4 respectively. The reference barrels were used to record the DC potentials and were filled with 0.15 M NaCl. In selected experiments, single barrel electrodes were also used in combination with single reference electrodes placed within 50 µm of each other. All ISMs were calibrated before and after each experiment using standard solutions (a < 5% difference was acceptable), and the calibration data were fitted to the Nikolsky equation to determine electrode slope and interference¹⁹. K⁺ and NH₄⁺ ISM traces were subtracted for ionic interference calculated by cross-calibrating the electrodes prior to use¹⁷. K⁺ calibrations were done in 150 mM NaCl that contained doubling steps of K⁺ over a range of concentrations appropriate for the experiment, usually from 3–48 mM. NH₄⁺ calibrations were carried out in 150 mM NaCl and aCSF from 0.1–10 mM to determine the sensitivity during the *in vivo* environment. H⁺ calibrations were carried out in phosphate buffers from pH 5 to 9, where > 90% had a response time of 1–5 s and a 51–59 mV response to 1 pH unit change.

Whole-cell and gramicidin perforated patch-clamp recordings were performed as described previously^{27,48}. Briefly, for whole-cell recordings we used electrodes with 3–5 M Ω resistance, and an intracellular solution containing: 135 mM K-methylsulfate, 10 mM KCl, 10 mM hepes, 5 mM NaCl, 2.5 mM Mg-ATP, 0.3 mM Na-GTP (pH 7.3), and Alexa Fluor® 350 (Invitrogen). Gramicidin perforated patch electrodes were filled with stock gramicidin (Sigma, 25 mg ml⁻¹ in DMSO), which was diluted to a final concentration of 50 μ g ml⁻¹ in solution containing: 130 mM KCl, 5 mM NaCl, 0.4 mM CaCl₂, 1 mM MgCl₂, 1.1 mM EGTA and 10 mM HEPES. Electroencephalogram (EEG) signals were externally filtered at 6 Hz (Filter Butterworth Model by Encore, Axopatch 200B by Axon Instruments), bandpass filtered at 1–100 Hz and digitized (Digidata 1440A by Axon Instruments). ISM signals were amplified (FD223a by WPI), externally filtered and digitized as above, and reference field potential traces were subtracted. In selected experiments, wireless electromyogram (EMG) and electroencephalogram (EEG) electrodes were implanted (DSI Physiotel®), and an extracellular microelectrode was placed in the thalamus (ventrobasal complex). Recordings were analyzed offline using pClamp 10.2. Myoclonic seizures were defined on the EEG as single or multiple 3–9 Hz polyspike and wave discharges (SWD) of 0.2–2 s duration associated with myoclonic jerks determined by video recording, EMG and direct observation. Whisker stimulation was delivered using a picospritzer III (Parken Instrumentation) and Master 8 (A.M.P.I.). Stimuli consisted of paired 50 μ s air pulses with an inter-stimulus interval of 150 ms, and paired-pulse ratio (PPR) was calculated as previously described²⁸. All solutions were pH (7.4) and osmolarity adjusted.

Two-photon laser scanning microscopy

A Mai Tai laser (SpectraPhysics) attached to a confocal scanning system (Fluoview 300, Olympus) and an upright microscope (IX51W) was used. *In vivo* volume changes and calcium activity were imaged in cortex 100 μ m below the pial surface as described before^{15,16}, using a 60x (1.1NA) and a 20x (0.95NA) lens, respectively. For *in vivo* volumetry we collected XYZT image series (z-step 1.5 μ m, every 5 min) with acquisition time < 20 s and laser power <40 mW. For *in vivo* calcium imaging we collected dual channel (rhod-2 and eGFP) frames at 0.2 or 1 Hz. A low sampling rate and <20 mW laser were also used here to avoid photodamage. A calcium transient was defined as an event where the relative ratio between the rhod-2 and eGFP signal intensities (F/F_0) was >2 standard deviations (σ) from baseline. Beginning and end were defined as $F/F_0 > 0.5 \sigma$ and $< 0.5 \sigma$ respectively. Amplitude was taken as the peak F/F_0 in this interval. For *in situ* volumetric imaging acute cortical slices were loaded with texas red hydrazide (1.5 μ M, a fixable sulforhodamine 101 derivative) in aCSF for 50 minutes. Volume and calcium recordings were analyzed using previously described custom-made software (MatLab Inc.)¹⁵.

Cell culture assays

Cultured neocortical astrocytes were prepared from P1-2 mouse and rat pups as previously described^{21,49}. For ⁸⁶Rb⁺ experiments the cultures were incubated for 10 min \pm ouabain (1 mM). The potassium analogue ⁸⁶Rb⁺ was then added to each well plate for 15 min (1 μ Ci, Perkin Elmer). The reaction was stopped by placing the cells on ice and washed with ice-cold aCSF. The cells were lysed and ⁸⁶Rb⁺ uptake quantified by liquid scintillation counting

(Beckman Coulter). For $\text{Na}^+\text{-K}^+\text{-ATPase}$ activity, astrocyte cultures were utilized as previously described, and enzyme activity was quantified using the malachite green reaction (Sigma) and analyzed using spectrophotometry⁵⁰.

Immunohistochemistry

Mice were anesthetized and perfused transcardially with 4% paraformaldehyde, and the brains were post-fixed overnight. Serial 16 μm sagittal cryostat sections were cut after overnight cryoprotection in 30% sucrose. Sections were incubated with goat anti-NKCC1 primary antibody (1:200, Sta. Cruz Biotechnology) overnight at 4°C, followed by incubation with an Alexa-488 donkey anti-goat secondary antibody (1:500, Invitrogen). Vectashield containing DAPI (Vector) was used for mounting. Images were taken with a 10x lens in a BX53 Olympus system microscope attached to a DP72 Olympus digital camera.

Biochemical and hemodynamic analyses

Plasma ammonia analysis was performed on blood samples collected using 50 μL heparinized tubes from the femoral artery. A L-glutamate dehydrogenase based kit (Sigma) was used for the quantification of ammonia in plasma⁵¹. For hemodynamic recordings an intracranial pressure probe (Millar) was inserted through a small 0.5 mm craniotomy over the somatosensory cortex. Cerebral blood flow was assessed using a fiberoptic laser Doppler probe (PF5010, Perimed) and connected to an infrared laser doppler flowmeter⁵². Blood pressure was monitored through the femoral artery cannula (SYS-BP1, WPI), and cerebral perfusion pressure was deduced by subtracting ICP from blood pressure⁵³. All signals were digitized (Digidata 1332A, Axon Instruments) and analyzed (pClamp 10.2). Brain water content was assessed using wet-to-dry ratios of brain weight as described previously⁵⁴. For $^1\text{H-NMR}$, mouse forebrains were extracted, frozen with liquid nitrogen, and homogenized in 7.5 mL 12% PCA at 0°C using a micro-sonicator. The homogenate was centrifuged at 25,000G for 15 minutes, and the supernatants were neutralized to pH 7.0 with KOH over an ice bath. A further 15-minute centrifugation (25,000G) separated the resultant KClO_4 , and the supernatant was lyophilized before being reconstituted with 0.65 ml $^2\text{H}_2\text{O}$, as described previously⁵⁵. $^1\text{H-NMR}$ spectra were acquired at 25°C using a 600 MHz Varian UnityINOVA spectrometer equipped with a triple-axis gradient HCN probe. Signals were acquired following a 90° pulse with a 7200 Hz spectral width and 32K data points. The time between pulses was 15 s and 64 signals were averaged for each spectrum. Integrals of the relevant peaks were converted to $\mu\text{mol}/\text{gram}$ wet-weight and normalized NAA (methyl) to increase inter-sample consistency.

Statistical analysis

All analysis was performed using SPSS 19 software (IBM) and all tests were two-tailed where significance was achieved at $\alpha = 0.05$ level. Where $n \geq 10$ for normally distributed data, an unpaired t test (≥ 2 variables) or ANOVA (> 2 variables) were used for independent samples, and paired t test for paired samples. Where $n < 10$ or the data was non-normally distributed we employed non-parametric tests including Mann-Whitney U (≥ 2 variables) or Kruskal-Wallis (> 2 variables) for independent samples, and Wilcoxon signed ranks test for

paired samples. Overdose survival was compared using a Cox regression model (controlling for the potential confounding effect of mouse weight and age).

Supplementary Material

Refer to Web version on PubMed Central for supplementary material.

Acknowledgments

We thank A.J. Cooper for discussion of the study, S. Kennedy for help with $^1\text{H-NMR}$ experiments, L.K. Bekar for help with electrophysiology, J. Chang for designing MatLab software, D. Wang for advice regarding electroencephalogram analysis, J.M. Wilson (University of Pennsylvania) for providing the *Otc^{spf-ash}* mice, J.D. Rothstein (Johns Hopkins University) for providing *Glt1*-eGFP BAC transgenic mice and C. Nicholson and S. Hrabetova for advice on fabrication and use of ion-sensitive electrodes. This work was supported by the US National Institutes of Health (grants NS078304 and NS078167 to M.N. and F31NS073390 to N.A.S.), Research Council of Norway (NevroNor FRIMEDBIO grants to E.A.N.), European Commission FP7-ICT-9-601055 to E.A.N., the Molecular Life Science program at the University of Oslo, the Letten Foundation and the Fulbright Foundation.

References

1. Cagnon L, Braissant O. Hyperammonemia-induced toxicity for the developing central nervous system. *Brain Res Rev.* 2007; 56:183–197. [PubMed: 17881060]
2. Cooper AJ. ^{13}N as a tracer for studying glutamate metabolism. *Neurochem Int.* 2011; 59:456–464. [PubMed: 21108979]
3. Butterworth RF. Pathophysiology of hepatic encephalopathy: a new look at ammonia. *Metab Brain Dis.* 2002; 17:221–227. [PubMed: 12602499]
4. Jayakumar AR, et al. Na-K-Cl Cotransporter-1 in the mechanism of ammonia-induced astrocyte swelling. *J Biol Chem.* 2008; 283:33874–33882. [PubMed: 18849345]
5. Ip YK, Chew SF. Ammonia production, excretion, toxicity, and defense in fish: a review. *Front Physiol.* 2010; 1:134. [PubMed: 21423375]
6. Marcaggi P, Jeanne M, Coles JA. Neuron-glia trafficking of NH_4^+ and K^+ : separate routes of uptake into glial cells of bee retina. *Eur J Neurosci.* 2004; 19:966–976. [PubMed: 15009144]
7. Waniewski RA. Physiological levels of ammonia regulate glutamine synthesis from extracellular glutamate in astrocyte cultures. *J Neurochem.* 1992; 58:167–174. [PubMed: 1345764]
8. Yamamoto Y, et al. Risk factors for hyperammonemia in pediatric patients with epilepsy. *Epilepsia.* 2013
9. Ye X, et al. Adenovirus-mediated in vivo gene transfer rapidly protects ornithine transcarbamylase-deficient mice from an ammonium challenge. *Pediatr Res.* 1997; 41:527–535. [PubMed: 9098855]
10. Rangroo Thrane V, et al. Real-time analysis of microglial activation and motility in hepatic and hyperammonemic encephalopathy. *Neuroscience.* 2012; 220:247–255. [PubMed: 22728097]
11. Ratnakumari L, Qureshi IA, Butterworth RF. Effects of congenital hyperammonemia on the cerebral and hepatic levels of the intermediates of energy metabolism in spf mice. *Biochem Biophys Res Commun.* 1992; 184:746–751. [PubMed: 1575747]
12. Martinez-Hernandez A, Bell KP, Norenberg MD. Glutamine synthetase: glial localization in brain. *Science.* 1977; 195:1356–1358. [PubMed: 14400]
13. Ratnakumari L, Audet R, Qureshi IA, Butterworth RF. Na^+ , K^+ -ATPase activities are increased in brain in both congenital and acquired hyperammonemic syndromes. *Neurosci Lett.* 1995; 197:89–92. [PubMed: 8552287]
14. Lichter-Konecki U, Mangin JM, Gordish-Dressman H, Hoffman EP, Gallo V. Gene expression profiling of astrocytes from hyperammonemic mice reveals altered pathways for water and potassium homeostasis in vivo. *Glia.* 2008; 56:365–377. [PubMed: 18186079]
15. Thrane AS, et al. Critical role of aquaporin-4 (AQP4) in astrocytic Ca^{2+} signaling events elicited by cerebral edema. *Proc Natl Acad Sci U S A.* 2011; 108:846–851. [PubMed: 21187412]

16. Thrane AS, et al. General anesthesia selectively disrupts astrocyte calcium signaling in the awake mouse cortex. *Proc Natl Acad Sci U S A*. 2012; 109:18974–18979. [PubMed: 23112168]
17. Stephan J, et al. Kir4.1 channels mediate a depolarization of hippocampal astrocytes under hyperammonemic conditions in situ. *Glia*. 2012; 60:965–978. [PubMed: 22431254]
18. Wall SM, Koger LM. NH₄⁺ transport mediated by Na(+)-K(+)-ATPase in rat inner medullary collecting duct. *Am J Physiol*. 1994; 267:F660–670. [PubMed: 7943362]
19. Nicholson C. Ion-selective microelectrodes and diffusion measurements as tools to explore the brain cell microenvironment. *J Neurosci Meth*. 1993; 48:199–213.
20. DeSalvo MN, et al. Focal BOLD fMRI changes in bicuculline-induced tonic-clonic seizures in the rat. *NeuroImage*. 2010; 50:902–909. [PubMed: 20079442]
21. Wang F, et al. Astrocytes modulate neural network activity by Ca²⁺(+)-dependent uptake of extracellular K⁺. *Sci Signal*. 2012; 5:ra26. [PubMed: 22472648]
22. Xiong ZQ, Stringer JL. Sodium pump activity, not glial spatial buffering, clears potassium after epileptiform activity induced in the dentate gyrus. *J Neurophysiol*. 2000; 83:1443–1451. [PubMed: 10712471]
23. Lux HD. Ammonium and chloride extrusion: hyperpolarizing synaptic inhibition in spinal motor neurons. *Science*. 1971; 173:555–557. [PubMed: 5564046]
24. Raabe W, Gumnit RJ. Disinhibition in cat motor cortex by ammonia. *J Neurophysiol*. 1975; 38:347–355. [PubMed: 1127446]
25. Szerb JC, Butterworth RF. Effect of ammonium ions on synaptic transmission in the mammalian central nervous system. *Prog Neurobiol*. 1992; 39:135–153. [PubMed: 1354386]
26. Dzhala VI, et al. NKCC1 transporter facilitates seizures in the developing brain. *Nat Med*. 2005; 11:1205–1213. [PubMed: 16227993]
27. Koyama R, et al. GABAergic excitation after febrile seizures induces ectopic granule cells and adult epilepsy. *Nat Med*. 2012
28. Borgdorff AJ, Poulet JF, Petersen CC. Facilitating sensory responses in developing mouse somatosensory barrel cortex. *J Neurophysiol*. 2007; 97:2992–3003. [PubMed: 17287446]
29. Rivera C, et al. The K⁺/Cl⁻ co-transporter KCC2 renders GABA hyperpolarizing during neuronal maturation. *Nature*. 1999; 397:251–255. [PubMed: 9930699]
30. Hubner CA, et al. Disruption of KCC2 reveals an essential role of K-Cl cotransport already in early synaptic inhibition. *Neuron*. 2001; 30:515–524. [PubMed: 11395011]
31. Delpire E, Lu J, England R, Dull C, Thorne T. Deafness and imbalance associated with inactivation of the secretory Na-K-2Cl co-transporter. *Nat Genet*. 1999; 22:192–195. [PubMed: 10369265]
32. Flagella M, et al. Mice lacking the basolateral Na-K-2Cl cotransporter have impaired epithelial chloride secretion and are profoundly deaf. *J Biol Chem*. 1999; 274:26946–26955. [PubMed: 10480906]
33. Raabe WA. Ammonia and disinhibition in cat motor cortex by ammonium acetate, monofluoroacetate and insulin-induced hypoglycemia. *Brain Res*. 1981; 210:311–322. [PubMed: 7013903]
34. Huberfeld G, et al. Perturbed chloride homeostasis and GABAergic signaling in human temporal lobe epilepsy. *J Neurosci*. 2007; 27:9866–9873. [PubMed: 17855601]
35. Hannaert P, Alvarez-Guerra M, Pirot D, Nazaret C, Garay RP. Rat NKCC2/NKCC1 cotransporter selectivity for loop diuretic drugs. *Naunyn Schmiedebergs Arch Pharmacol*. 2002; 365:193–199. [PubMed: 11882915]
36. Benjamin AM. Effects of ammonium ions on spontaneous action potentials and on contents of sodium, potassium, ammonium, and chloride ions in brain in vitro. *J Neurochem*. 1978; 30:131–143. [PubMed: 621504]
37. Dzhala VI, et al. Progressive NKCC1-dependent neuronal chloride accumulation during neonatal seizures. *J Neurosci*. 2010; 30:11745–11761. [PubMed: 20810895]
38. Kanaka C, et al. The differential expression patterns of messenger RNAs encoding K-Cl cotransporters (KCC1,2) and Na-K-2Cl cotransporter (NKCC1) in the rat nervous system. *Neuroscience*. 2001; 104:933–946. [PubMed: 11457581]

39. Javaheri S, Davis C, Rogers DH. Ionic composition of cisternal CSF in acute respiratory acidosis: lack of effect of large dose bumetanide. *J Neurochem.* 1993; 61:1525–1529. [PubMed: 8377001]
40. Regan MR, et al. Variations in promoter activity reveal a differential expression and physiology of glutamate transporters by glia in the developing and mature CNS. *J Neurosci.* 2007; 27:6607–6619. [PubMed: 17581948]
41. Guyenet SJ, et al. A simple composite phenotype scoring system for evaluating mouse models of cerebellar ataxia. *J Vis Exp.* 2010
42. Matkowskyj KA, et al. Azoxymethane-induced fulminant hepatic failure in C57BL/6J mice: characterization of a new animal model. *Am J Physiol.* 1999; 277:G455–G462. [PubMed: 10444460]
43. Han X, et al. Forebrain engraftment by human glial progenitor cells enhances synaptic plasticity and learning in adult mice. *Cell stem cell.* 2013; 12:342–353. [PubMed: 23472873]
44. Anagnostaras SG, Josselyn SA, Frankland PW, Silva AJ. Computer-assisted behavioral assessment of Pavlovian fear conditioning in mice. *Learn Mem.* 2000; 7:58–72. [PubMed: 10706603]
45. Wiltgen BJ, Silva AJ. Memory for context becomes less specific with time. *Learn Mem.* 2007; 14:313–317. [PubMed: 17522020]
46. Dombeck DA, Khabbaz AN, Collman F, Adelman TL, Tank DW. Imaging large-scale neural activity with cellular resolution in awake, mobile mice. *Neuron.* 2007; 56:43–57. [PubMed: 17920014]
47. Thrane VR, et al. Real-time analysis of microglial activation and motility in hepatic and hyperammonemic encephalopathy. *Neuroscience.* 2012
48. Wang F, Xiao C, Ye JH. Taurine activates excitatory non-synaptic glycine receptors on dopamine neurones in ventral tegmental area of young rats. *J Physiol.* 2005; 1:503–516. [PubMed: 15817633]
49. Lin JH, et al. Gap-junction-mediated propagation and amplification of cell injury. *Nat Neurosci.* 1998; 1:494–500. [PubMed: 10196547]
50. Anupama Adya HV, Mallick BN. Comparison of Na-K ATPase activity in rat brain synaptosome under various conditions. *Neurochem Int.* 1998; 33:283–286. [PubMed: 9840218]
51. Mondzac A, Ehrlich GE, Seegmiller JE. An enzymatic determination of ammonia in biological fluids. *J Lab Clin Med.* 1965; 66:526–531. [PubMed: 4284306]
52. Takano T, et al. Cortical spreading depression causes and coincides with tissue hypoxia. *Nat Neurosci.* 2007; 10:754–762. [PubMed: 17468748]
53. Ren Z, et al. ‘Hit & Run’ model of closed-skull traumatic brain injury (TBI) reveals complex patterns of post-traumatic AQP4 dysregulation. *J Cereb Blood Flow Metab.* 2013; 33:834–845. [PubMed: 23443171]
54. Haj-Yasein NN, et al. Glial-conditional deletion of aquaporin-4 (Aqp4) reduces blood-brain water uptake and confers barrier function on perivascular astrocyte endfeet. *Proc Natl Acad Sci U S A.* 2011; 108:17815–17820. [PubMed: 21990350]
55. Zwingmann C, Chatauret N, Leibfritz D, Butterworth RF. Selective increase of brain lactate synthesis in experimental acute liver failure: results of a [¹H-¹³C] nuclear magnetic resonance study. *Hepatology.* 2003; 37:420–428. [PubMed: 12540793]

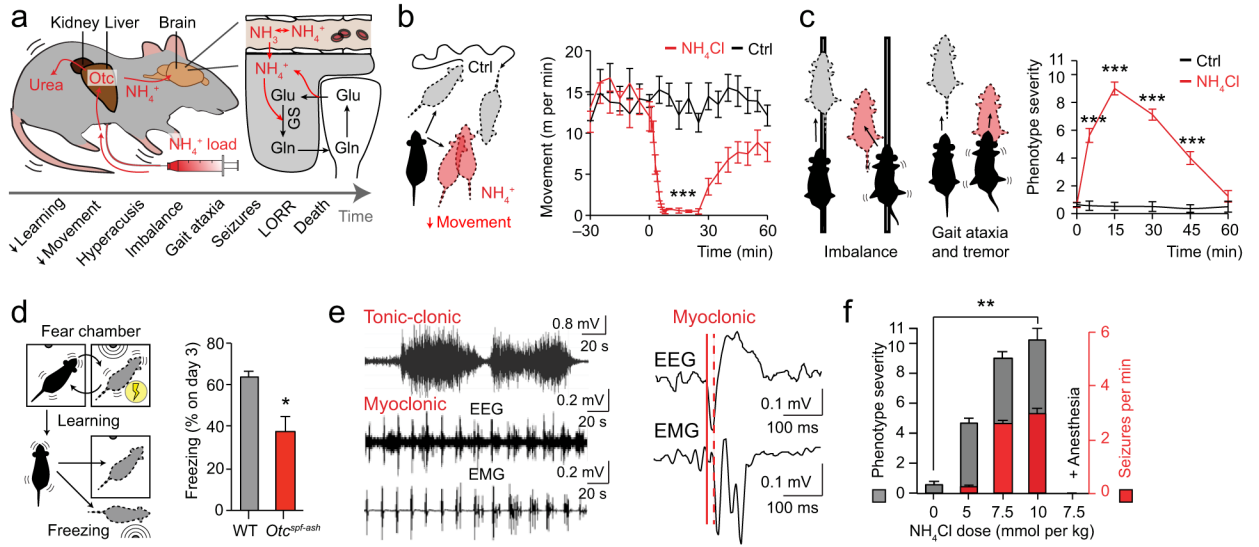


Figure 1.

Ammonia neurotoxicity causes severe neurological impairment and seizures. **(a)** Diagram showing *Otc^{spf-ash}* mouse model of acute ammonia neurotoxicity. Ornithine transcarbamylase (*Otc*), glutamine synthetase (*GS*), glutamate (*Glu*), glutamine (*Gln*), loss of righting reflex (*LORR*). **(b)** Automated movement analysis of *Otc^{spf-ash}* mice given a systemic ammonia load (7.5 mmol kg⁻¹) and saline controls (*n* = 5–8). **(c)** Phenotype severity score at different time points after ammonia (*n* = 8) or saline (*n* = 5) load in *Otc^{spf-ash}* mice at time 0. **(d)** Percent animal freezing on day 3 of spatial fear conditioning comparing *Otc^{spf-ash}* (*n* = 5) and wild-type (*WT*, *n* = 5) mice. **(e)** Representative electroencephalogram (EEG) and electromyogram (EMG) recordings of tonic-clonic and myoclonic seizures in ammonia-exposed *Otc^{spf-ash}* animals (*n* = 10). **(f)** Phenotype severity (grey, left axis) compared to myoclonic seizure frequency (red, right axis) with increasing doses of ammonia in *Otc^{spf-ash}* mice (*n* = 6 for each). **P* < 0.05, ***P* < 0.01, ****P* < 0.001. Data are shown as mean ± SEM.

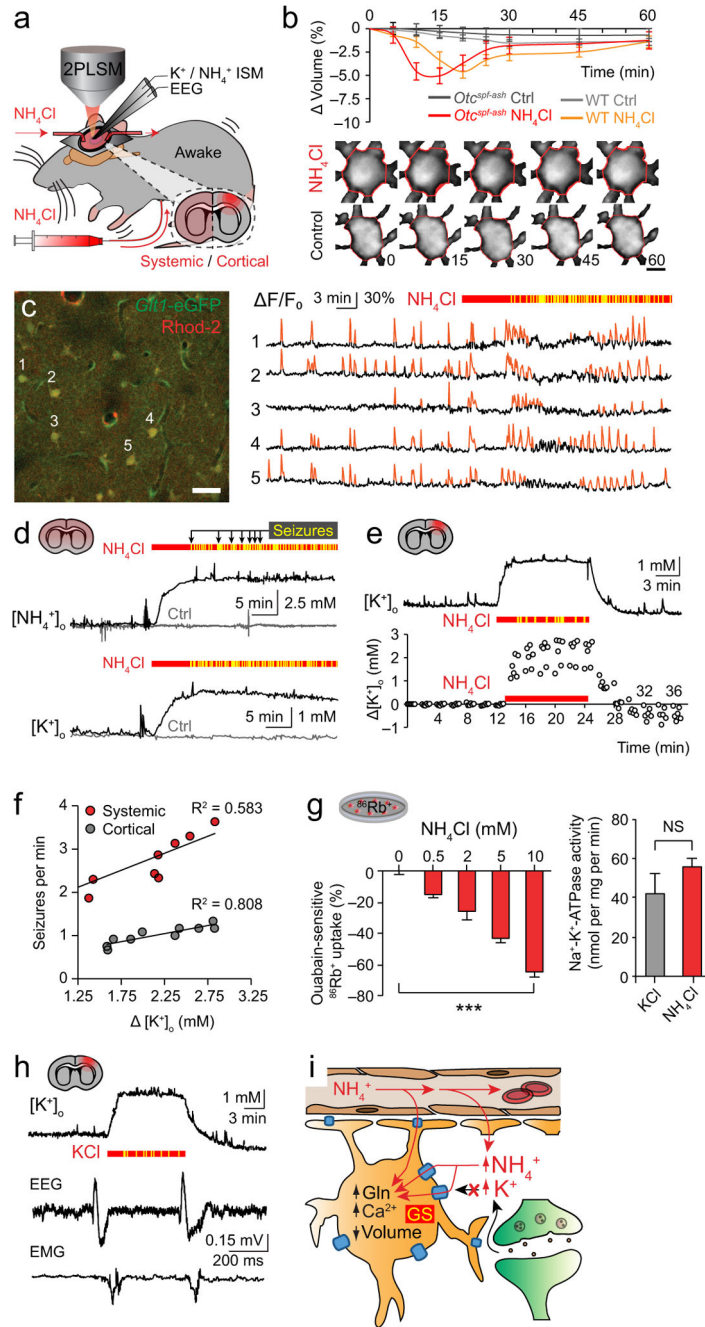


Figure 2. Ammonia compromises astroglial potassium buffering by competing for uptake. (a) Experimental set-up for studying systemic and cortical ammonia neurotoxicity. 2-photon laser-scanning microscopy (2PLSM), electroencephalogram (EEG). (b) Top, volume analysis of enhanced green fluorescent protein (eGFP) expressing astrocytes during ammonia neurotoxicity ($n = 12$ for each). Bottom, representative auto-thresholded images (red outline = volume at time 0). Scale bar 5 μm . (c) Left, representative image of eGFP-expressing astrocytes loaded with calcium indicator rhod-2. Scale bar 30 μm , depth 100 μm .

Right, corresponding rhod-2 intensity traces (F/F_0 , eGFP-normalized) before and after a systemic ammonia load (red bar) in *Otcspf-ash* mouse. **(d)** Representative NH_4^+ (top) and K^+ (bottom) recordings following systemic ammonia (red bar) or saline (control) load in *Otcspf-ash* mice. **(e)** Representative K^+ trace (top) and scatterplot of all recordings (bottom, $n = 7-10$) after cortical application of ammonia (10 mM, red bar). **(f)** Linear regression of myoclonic seizure frequency on peak cortical $[\text{K}^+]_o$ during systemic and cortical ammonia neurotoxicity ($n = 8-10$). **(g)** Left, ouabain-sensitive rubidium ($^{86}\text{Rb}^+$) uptake in cultured astrocytes exposed to ammonia, normalized to vehicle ($n = 10-23$). Right, $\text{Na}^+-\text{K}^+-\text{ATPase}$ activity measured in 15 mM KCl or NH_4Cl solution using a cell-free assay of astrocytes ($n = 4$ for each). **(h)** Representative recordings of K^+ (top) and myoclonic seizures (bottom) during cortical KCl application (red bar, 12.5 mM, $n = 6$). Electromyogram (EMG). **(i)** Diagram of how anatomical (end-feet) and enzymatic (glutamine synthetase, GS) trapping of ammonia in astrocytes compromises their ability to buffer potassium. Glutamine, Gln. Individual myoclonic seizures are indicated by yellow bars throughout. * $P < 0.05$, ** $P < 0.01$, *** $P < 0.001$, not significant (NS). Data are shown as mean \pm SEM.

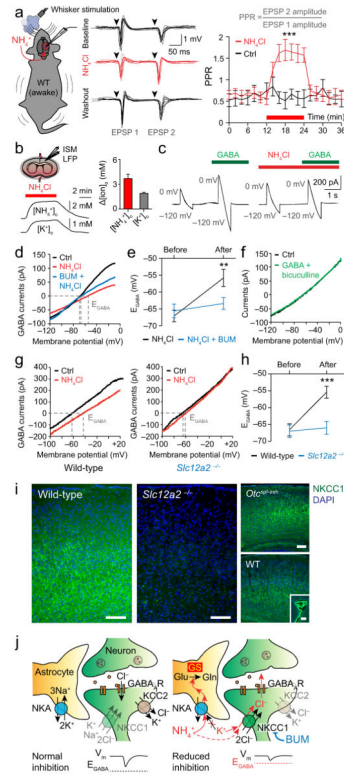


Figure 3.

Excess ammonia and potassium depolarize the neuronal GABA reversal potential (E_{GABA}) via neuronal $Na^+-K^+-2Cl^-$ -cotransporter 1 (NKCC1). **(a)** Left, diagram of whisker stimulation recordings. Middle, 10 consecutive field excitatory post-synaptic potentials (EPSP) before, during (red) and after cortical ammonia application (10 mM) in wild-type (WT) mice. Right, paired-pulse ratio (PPR) during cortical ammonia application (red bar) and in controls ($n = 10$ for each). **(b)** Left, diagram of cortical slice superfused with ammonia (top), and representative ion-sensitive microelectrode (ISM) recordings (bottom). Right, change in ion concentration with 7.5 mM ammonia superfusion ($n = 9-18$). **(c)** Representative whole-cell current recordings from pyramidal neurons during ramp voltage, before vs. after GABA \pm ammonia application. **(d)** Current-voltage (I-V) curve comparing effect of ammonia \pm bumetanide (BUM) on the currents induced by GABA applications ($n = 7-11$). **(e)** Mean E_{GABA} shift caused by ammonia \pm bumetanide ($n = 7-11$). **(f)** I-V curve of bicuculline and GABA co-application. **(g)** I-V curve for gramicidin perforated patch recordings before vs. after ammonia exposure in wild-type (left) and *Slc12a*^{-/-} (right) mice ($n = 6-7$). **(h)** Ammonia-induced E_{GABA} shift in wild-type and *Slc12a*^{-/-} mice ($n = 6-7$). **(i)** Immunofluorescence micrographs of *Slc12a*^{-/-}, *Otc*^{spf-ash} and wild-type mouse cortex labeled for NKCC1 (green) and nuclei (blue, DAPI). Inset shows choroid plexus. Scale bars 100 μm . **(j)** Diagram of proposed disease mechanism. $Na^+-K^+-ATPase$ (NKA), glutamate (Glu), glutamine synthetase (GS), glutamine (Gln), GABA_A receptor (GABA_AR), K^+-Cl^- cotransporter isoform 2 (KCC2), membrane potential (V_m). $**P < 0.01$, $***P < 0.001$. Data are shown as mean \pm SEM.

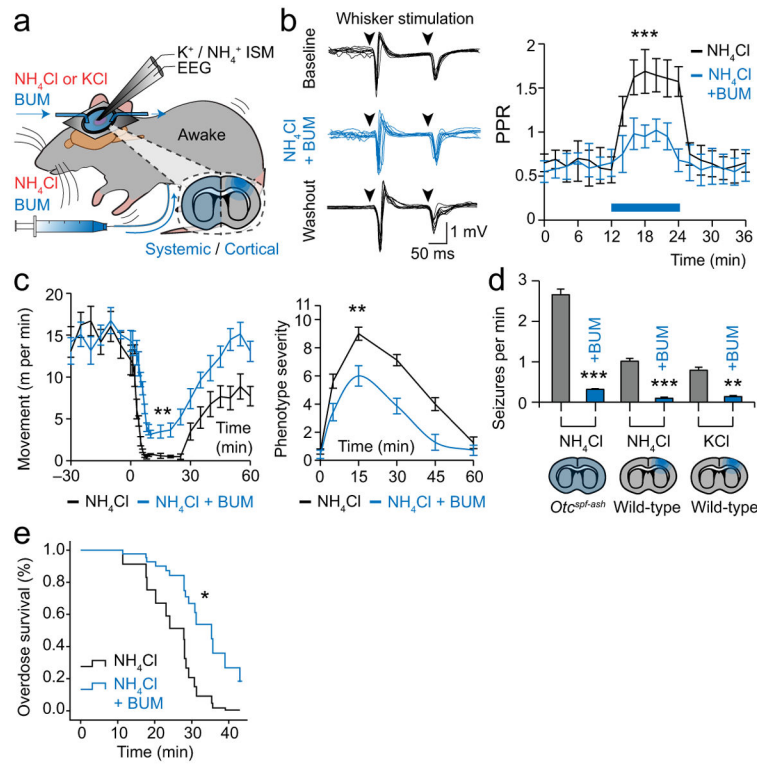


Figure 4. Inhibiting $Na^+K^+-2Cl^-$ cotransporter 1 (NKCC1) with bumetanide treats the electrophysiological and clinical features of ammonia neurotoxicity. **(a)** Diagram showing bumetanide treatment (BUM, 30 mg kg^{-1} or $5 \mu\text{M}$) for systemic and cortical models of ammonia neurotoxicity. **(b)** Left, 10 consecutive field recordings during paired-pulse whisker stimulation shown before, during (blue), and after cortical application of ammonia with bumetanide. Right, change in paired-pulse ratio (PPR) following cortical ammonia application (blue box) with bumetanide ($n = 10$ for each). **(c)** Automated mouse movement analysis (left) and phenotype severity score (right) after a systemic ammonia load (at time 0) in $Otc^{spf-ash}$ mice with bumetanide treatment ($n = 7-8$). **(d)** Effect of bumetanide on myoclonic seizure frequency induced by ammonia and potassium neurotoxicity ($n = 6-10$). **(e)** Cox regression of $Otc^{spf-ash}$ mouse survival time after an ammonia overdose (10 mmol kg^{-1} , $n = 9-10$). * $P < 0.05$, ** $P < 0.01$, *** $P < 0.001$. Data are shown as mean \pm SEM.